Manipulation of ultrafast demagnetization dynamics by optically induced intersite spin transfer in magnetic compounds with distinct density of states

Martin Borchert,[1] Clemens von Korff Schmising,[1] Daniel Schick,[1] Dieter Engel,[1] Sangeeta Sharma,[1] and Stefan Eisebitt[1,2]

[1] *Max-Born-Institut für Nichtlineare Optik und Kurzzeitspektroskopie, 12489 Berlin, Germany*
[2] *Technische Universität Berlin, Institut für Optik und Atomare Physik, Straße des 17. Juni 135, 10623 Berlin*

(Dated: August 31, 2020)

Optical control of magnetization dynamics on a femtosecond time scale is of relevance for the improvement of future, fast and energy-efficient magnetic storage media. Here, we present a systematic comparison of the ultrafast magnetic response between the *3d* ferromagnets (FMs), Fe, Co, and Ni, and their respective Pt-based alloys and multilayers (MLs) to provide new insights into the recently theoretically predicted optically induced intersite spin transfer (OISTR). In the FMPt alloys and FM|Pt MLs optical laser excitation leads to a spin current dominated by minority carriers from the Pt to the FM sublattice, significantly enhancing the efficiency of the demagnetization amplitude. We propose this transfer to be dependent on the number of available, unoccupied states at the spin-drain (FM sublattice) and show a quantitative correlation between the number of unoccupied minority *3d* states above the Fermi level of each FM and the respective enhancement of the demagnetization amplitude upon adding Pt as a spin donor. We provide support for this hypothesis by magneto-optical Kerr effect measurements with femtosecond time resolution, as well as by *ab-initio* simulations based on time-dependent density functional theory. Our study widens the path towards density of states-engineering in order to actively influence the demagnetization efficiency, especially on, but not limited to, timescales below one hundred femtoseconds.

I. INTRODUCTION

To cope with the ever-increasing demand in data storage and processing, all-optical technologies are emerging as new and promising concepts to provide faster and more energy-efficient manipulation of units of information. Research, investigating ultrafast optical control of magnetization, has made a lot of progress since its first discovery[1]: the magnetization of ferrimagnetic[2,3] or antiferromagnetic materials[4] can be deterministically reversed; spin currents can be launched [5,6], injected into a non-magnetic material[7,8] and result in efficient THz emission[9,10].

A completely new concept to change the magnetic state with an optical laser pulse was recently proposed theoretically by Dewhurst et al.[11]. Here, optical laser pulses induce a spin-selective intersite charge flow in multicomponent magnetic systems and can drive a transition between antiferromagnetic and ferromagnetic order. It is named optically induced intersite spin transfer (OISTR). This transfer between two distinct sites S (spin source) and D (spin drain) within a magnetic material takes place on ultrashort time scales and changes the *local* magnetization without the necessity for spin flips, which would require additional energy to occur. The efficiency and directionality of OISTR crucially depends on an asymmetry of the density of states (DOS) at S and D. If the D site is characterized by an excess of available, unoccupied minority *3d* states above the Fermi level, OISTR is expected to be dominated by transfer of minority carriers. Consequently, an equalization of majority and minority spins at D leads to a loss in its *local* magnetization, while a loss of minority states at S will lead to a *local* increase in its magnetization.

Experimental verification of OISTR was recently shown for a select number of different multi-component magnetic materials: on the one hand via optical spectroscopy for CoCu by Chen et al.[12] as well as in half-Heusler materials by Steil et al.[13], and on the other hand by time-resolved resonant spectroscopy in the extreme ultraviolet spectral range for NiPt by Siegrist et al.[14], for Co_2MnGe by Tengdin et al.[15], in FeNi by Hofherr et al.[16] and in CoPt by Willems et al.[17].

While probing core-to-valence band transitions in resonant spectroscopy has been shown to be sensitive to element-specific, transient occupation changes within the DOS and, hence, to a spin-dependent accumulation of electrons at a distinct site[17], such experiments in the extreme ultraviolet spectral range are still very challenging. Thus, systematic studies for an extensive number of samples in a large fluence range are missing in literature.

Here, we test the hypothesis whether tailoring the number of available, unoccupied states in two-component magnetic systems allows to directly influence the efficiency of ultrafast demagnetization. To this end, we carried out a systematic comparison of the demagnetization dynamics between the three *3d* ferromagnets (FMs) (Fe, Co, and Ni) and their respective FMPt alloys and FM|Pt multilayers (MLs) within the same experimental setup and under the same excitation conditions.

We performed optical pump - probe magneto-optical Kerr effect (MOKE) measurements to determine the relative demagnetization amplitudes, A, of all *3d* FMs and of their respective FM|Pt MLs (and FMPt alloys) over a wide range of excitation fluences. The ratio of A between the pure FMs and the FM|Pt MLs (and FMPt alloys) scales with the number of available, unoccupied minority states above the Fermi level in the respective

FM: we find the largest value of the ratio for Fe to Fe|Pt, a slightly smaller one for Co to Co|Pt and a significantly smaller one for Ni to Ni|Pt MLs.

II. HYPOTHESIS

The excitation of an FM by an optical pump laser pulse leads to a non-equilibrium occupancy distribution of minority and majority spins. Spin-flip scattering, mediated by spin-orbit coupling, leads to a quenching of the magnetization, as the number of minority and majority spins equalize and compensate each other. This process is fundamentally limited by the intrinsic energy of spin-orbit coupling in the FM[18].

If an additional element (e.g. Pt), exhibiting a distinct DOS, is added to the FM, OISTR, as an additional spin-transfer channel, becomes available for demagnetization. We show the projected DOS for the three different FMs inside their respective FMPt alloys in Fig. 1. Upon laser excitation of the compound, electrons carrying minority spins of Pt can transfer into empty minority states of the adjacent *3d* orbitals of the FM. Here they compensate the majority spins, thus quenching the *local* magnetization of the FM. In combination with a strong spin-orbit coupling localized on Pt and a concomitant stronger spin-flip probability[17,19] the demagnetization amplitude A should be higher in the FMPt alloy and in the FM|Pt ML than in the respective pure FM due to the absence of this channel in the latter one. Note that in the 50%:50% FMPt alloy and FM|Pt ML *both* elements have an unequal amount of majority and minority spins below the Fermi level, i.e. ferromagnetic atoms at S induce a finite net magnetic moment at their neighboring D sites.

For the case of a CoPt alloy this theory has been successfully put to the test in a recent work of Willems et al., where element-specific magnetic circular dichroism spectroscopy in the extreme ultraviolet range and helicity-dependent resonant transient absorption was combined to demonstrate the transfer of minority carriers from Pt to Co.[17]. Guided by *ab-initio* time-dependent density functional theory (TDDFT) calculations, it was shown that the early time dynamics are indeed dominated by OISTR together with spin-orbit-coupling-driven spin-flips locally at the Pt atom. Importantly, the number of available states emerged as the driver of the OISTR process in Co. This forms the basis for our main hypothesis, namely that the ratios of the demagnetization efficiencies scale with the ratios of available, unoccupied *3d* states of the different FMs within the alloys and MLs.

To investigate this proposed dependency, we keep S the same (Pt), but vary the number of available, unoccupied states at D by comparing different FMPt alloys and FM|Pt MLs.

To quantify the number of available, unoccupied minority *3d* states, and therefore the expected increase in A between the FM and its respective FMPt alloy, we sum the relevant *3d* states from the electronic structure calculations as a function of the energy $E' = E - E_F$ and show the result in Fig. 2. Due to non-linear excitation, electrons can gain energy in excess of the photon energy $E_p = 1.55\,\text{eV}$ of the pump pulse[17], thus we show the sum up to an energy of $E' = 4\,\text{eV}$. Note, that for $E' > 1.55\,\text{eV}$ the free states of Fe are ≈1.4 larger than those of Co and ≈3.2 times larger than those of Ni. We can therefore formulate our hypothesis as follows: the ratios of the demagnetization amplitudes A for the different FMs and their respective FMPt alloys are postulated to follow the

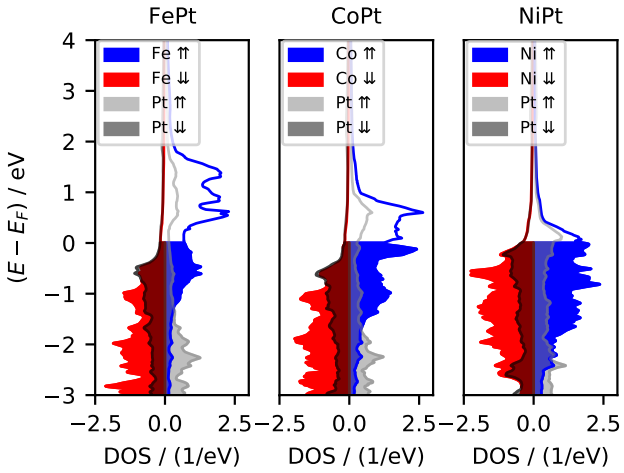

Figure 1. **Calculated density of states for *3d*-orbitals of Fe, Co, Ni, as well as the *5d*-orbitals of Pt inside the respective FMPt alloys.** Majority states in red (FM)/ dark gray (Pt) and minority states in blue (FM)/ light gray (Pt). During the OISTR process minority spins from Pt can transfer into the empty minority *3d*-states of the respective FM, where they compensate the majority spins and the magnetization quenches. This process should be dependent on the number of available *3d*-states in the FM.

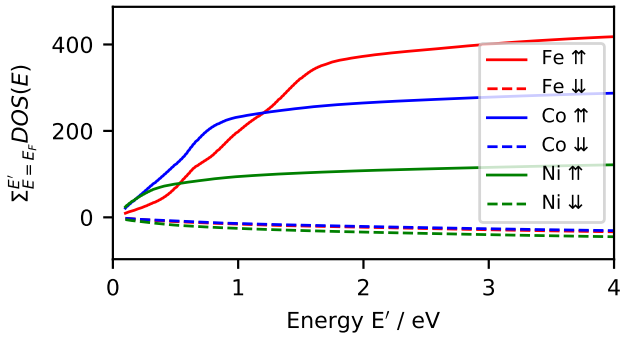

Figure 2. **Sum of available, unoccupied *d*-states of different FMs in FMPt alloys summed up to the energy E above E_F for minority (⇈) and majority (⇊) spins.** Above E = 1.55 eV the summed number of states for Fe is ≈ 1.4 larger than for Co and ≈ 3.2 times larger than for Ni.

relative difference in available, unoccupied states, i.e.:

$$\frac{A(\mathrm{FePt})}{A(\mathrm{Fe})} \approx 1.4 \frac{A(\mathrm{CoPt})}{A(\mathrm{Co})} \approx 3.2 \frac{A(\mathrm{NiPt})}{A(\mathrm{Ni})}. \quad (1)$$

We note that these relations represent simple estimates and are understood as an intuitive description; later we compare this hypothesis with *ab-initio* TDDFT simulations, taking into account the full transition probabilities. In the following, we put this hypothesis to the test by performing systematic optical pump-probe MOKE measurements in order to compare the magnetization dynamics of pure FM thin films and their respective FMPt alloy or FM|Pt ML thin films. We compare our results with *ab-initio* simulations based on TDDFT.

III. EXPERIMENTAL SETUP

We used the well-established MOKE technique in a pump-probe geometry to measure the ultrafast magnetization dynamics. The MOKE describes changes to light upon reflection off a magnetized material. In a polar (P-MOKE) or longitudinal (L-MOKE) geometry, the polarization plane of linearly-polarized light is rotated and partially turned elliptical upon the reflection. Both effects are proportional to the component of the magnetization parallel to the propagation direction of the incident light. A schematic of our setup is shown in Fig. 3.

The sensitivity of MOKE measurements relies on a high degree of linear polarization of the probe pulse, which we achieve by a set of four reflection polarizers. With a pulse duration of 39 fs (FWHM) of the pump (λ_{pump} = 800 nm) and probe (λ_{probe} = 400 nm) pulses, we measure a corresponding cross-correlation between the two pulses of σ = 55 fs, defining the overall temporal resolution of the experiment. To conserve this high time resolution, pump and probe beams are kept collinear to within a few degrees and transmissive optics are avoided whenever possible. To suppress coherent artifacts[20], the pump beam is set to *p*-polarization, where the probe beam is kept in *s*-polarization.

By rotating a $\lambda/2$ wave plate, which sets the *s*- and *p*-components of the light in front of the subsequent reflective *p*-polarizer, we vary the incident fluence on the sample between 0.5 mJ/cm^2 and 20 mJ/cm^2. We determine the absolute values of the absorbed fluence by careful measurements of the pump spot footprints (for different angles of incidence ($\approx 26°$ for L-MOKE and $\approx 0°$ for P-MOKE) at the sample position with a calibrated beam profiler camera and by determining the transmitted (a few percent) and the reflected (50-70%) pump power.

After reflection off the sample, the probe beam is split into its *s*- and *p*-components by a Wollaston prism and their differential intensity is detected by a balanced photo diode. This signal is, to first order, directly proportional to the Kerr rotation and therefore to the magnetization. To determine the absolute value of the laser-induced magnetization change for each time delay between the pump and probe pulses, we toggle the magnetic field between the saturation field B_{sat} and $-B_{\mathrm{sat}}$ of the respective sample and measure the corresponding transient MOKE signal at a 3 kHz repetition rate. The difference between these two signals is proportional to the transient magnetization $M(t)$. By following this procedure, we also subtract out any non-magnetic contributions from the signal. To increase the signal-to-noise ratio, for every other probe pulse we block the pump pulse with a mechanical chopper and record the signal by a lock-in-amplifier-based, digital box-car integrator. Finally, we normalize our data to unity for delay points before time zero, yielding the relevant observable $M(t)/M_0$, where $M_0 = M(t < 0)$.

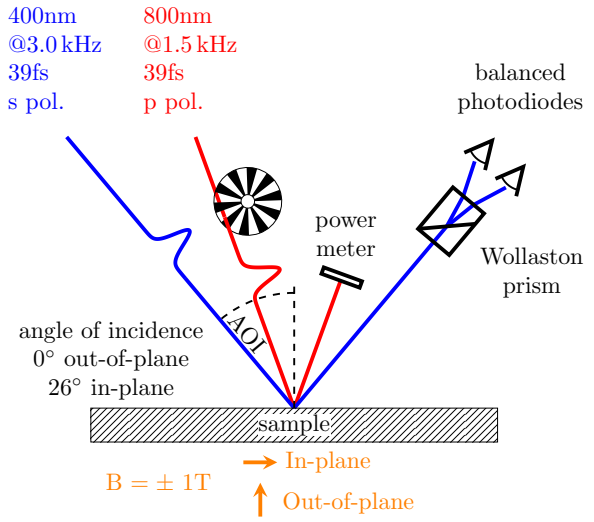

Figure 3. **Setup for measuring the magnetization via the longitudinal (L-) or polar (P-) MOKE**. The plane of polarization of the incident optical probe pulses (blue line) is rotated upon reflection off a magnetic sample. This translates into a relative intensity change after transmission through a Wollaston prism and is detected by balanced photo diodes, yielding a signal proportional to the magnetization. The pump pulses arrive at the sample at a known, tunable time delay. The incident, transmitted (not shown) and reflected pump power is measured during the experiment. The sample can be magnetized in-plane (L-MOKE) and out-of-plane (P-MOKE) of the sample with an external magnetic field of up to 1 T.

A high degree of automation of the relevant optomechanical components, e.g. the $\lambda/2$ wave plate to set the incident fluence, the mirrors that control the spatial pump-probe overlap and the delay stage, allow for continuous, systematic measurements for a large number of different parameters without human interference.

We prepared pure FM thin films Fe(15), Co(15), and Ni(15), their respective alloys $\mathrm{FM_{50}Pt_{50}}(15)$, as well as MLs Pt(2)|[FM(d_{FM})|Pt(0.2)] × 30 with d_{Fe} = 0.15, d_{Co} = 0.14, and d_{Ni} = 0.50. All film thicknesses (in parentheses) are given in nanometers. Note that because $\mathrm{Ni_{50}Pt_{50}}$ alloys do not form a ferromagnetic phase

at room temperature[21], we only investigated the FePt and CoPt alloys.

All samples are magnetron-sputtered on glass wafers. The pure FMs, as well as the alloys exhibit an in-plane magnetic anisotropy and have been capped with 2 nm of Ta to prevent oxidation. The MLs show a strong out-of-plane anisotropy and have been seeded and capped with 2 nm of Pt. The hysteresis curves are shown in the Supplementary Material[22].

IV. RESULTS

In Fig. 4 we present the normalized de- and remagnetization dynamics $M(t)/M_0$ for the three pure FMs. The data points are shown as dots, fits as solid lines; note that the x-axis is divided into a linear scale up to 1 ps and a logarithmic scale after 1 ps in order to also capture the different remagnetization dynamics. We further show the same measurements but for the respective Pt alloys in Fig. 5 and MLs in Fig. 6. All data thus far is shown for the given *incident* fluences.

In Fig. 7, we present exemplary measurements that correspond to an *absorbed* fluence of $\approx 4\,\mathrm{mJ/cm^2}$, accounting for different transmission and reflection, as mentioned above. Despite an almost identical absorbed fluence, we observe very different dynamics for the different samples, both in terms of the maximal amplitude and temporal evolution of the magnetization: Fe demagnetizes by only approximately 10% and exhibits a slow recovery. Co demagnetizes slightly more, but rapidly recovers its magnetization (note that the oscillations visible in Figs. 4 and 7 can be attributed to the excitation of acoustic strain waves in the thin Co layer[23], cf. footnote[24]) Ni shows the largest response and loses almost 80% of its initial magnetization.

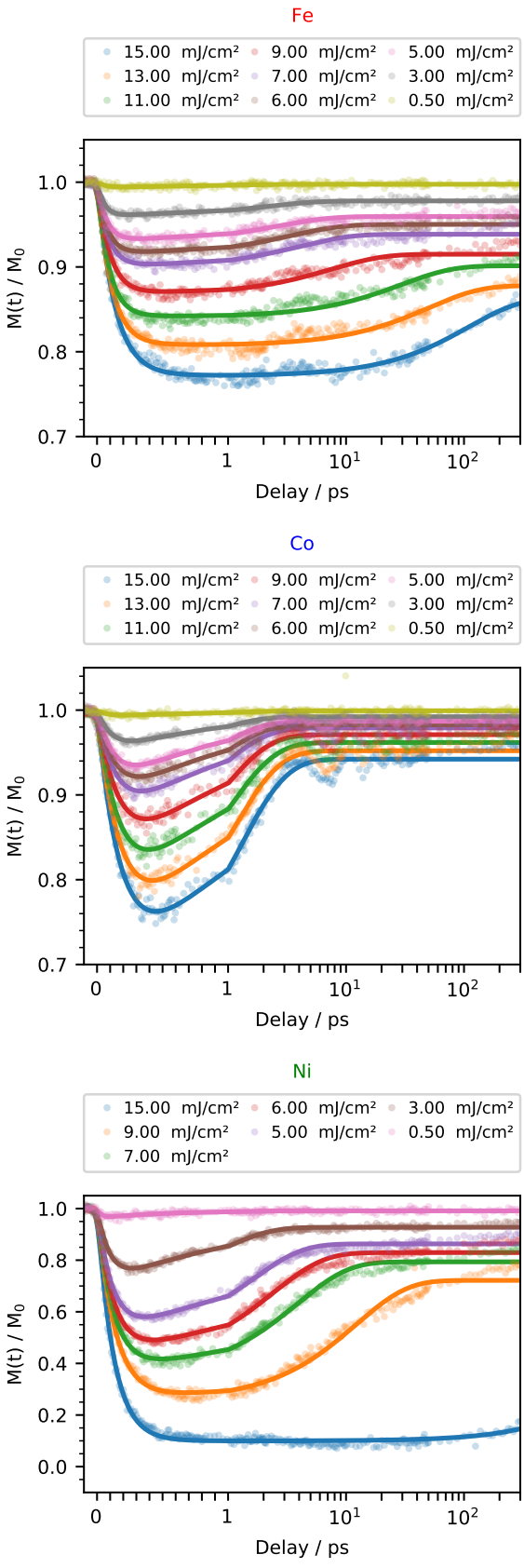

Figure 4. **Normalized magnetization ($M(t)/M_0$) for different incident fluences onto the pure FM thin films.** The x-axis is linear up to 1 ps and logarithmic afterwards. Measured in in-plane geometry. Top: Fe, middle: Co, bottom: Ni

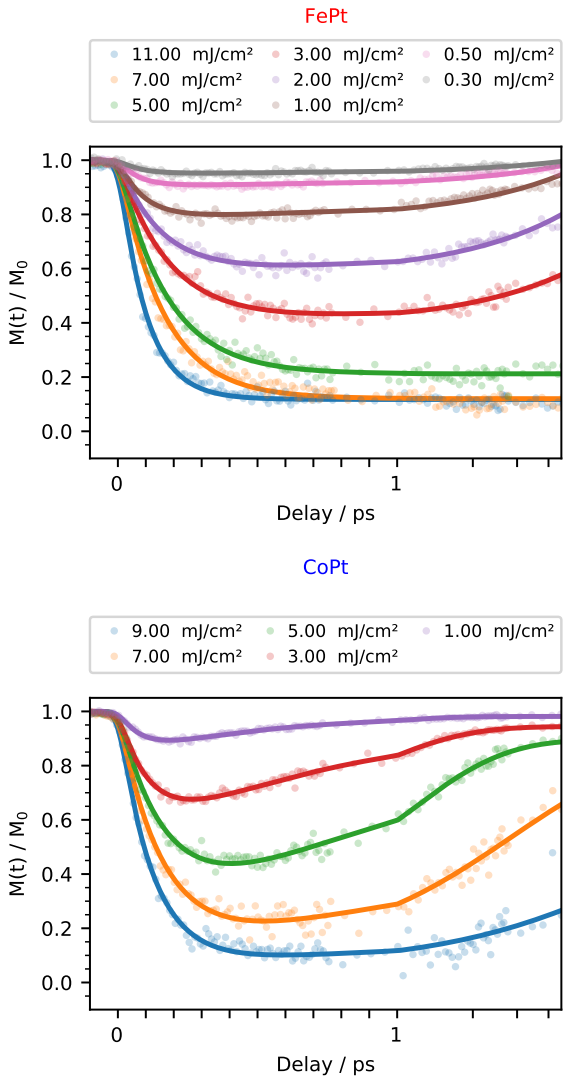

Figure 5. **Normalized magnetization ($M(t)/M_0$) for different incident fluences onto the FMPt alloys.** The x-axis is linear up to 1 ps and logarithmic afterwards. Measured in in-plane geometry. Top: FePt alloy, bottom: CoPt alloy

The magnetization of all FM|Pt MLs is fully quenched at the excitation fluence of $\approx 4\,\mathrm{mJ/cm^2}$, however the minimum is reached on slightly different time scales. We note that the Co|Pt ML demagnetizes more than 100%, which is likely due to errors of the normalization due to small DC-heating of the samples. Also this sample requires a large saturation magnetic field of almost 1 T, which may lead to parasitic Faraday rotations.

To extract A, we describe $M(t)/M_0$ by a double exponential fit function, convolved by a Gaussian function with the full width at half maximum (FWHM) corresponding to the measured cross-correlation FWHM $= 2\sqrt{2\log(2)}\sigma = 55\,\mathrm{fs}$:

$$M(t) = \int_{-\infty}^{\infty} d\xi e^{-\xi^2/2\sigma^2} \left(Ae^{-t-\xi/\tau_1} + Be^{-t-\xi/\tau_2}\right)\theta\left(t-\xi\right).$$

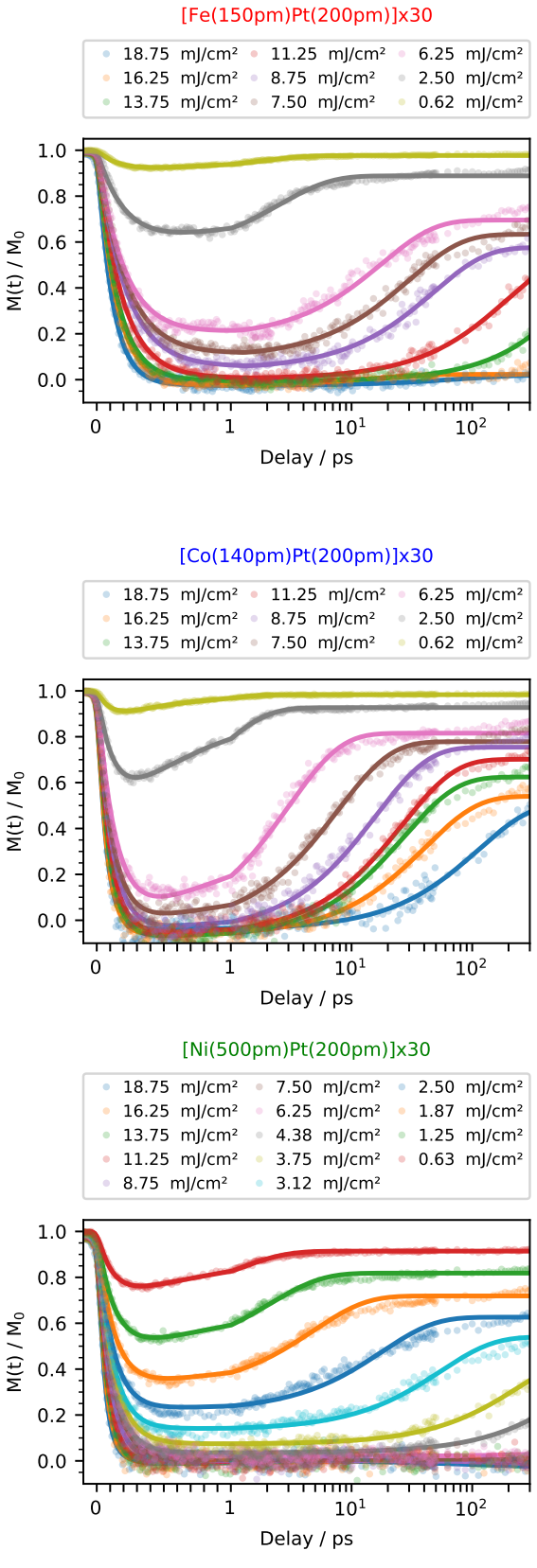

Figure 6. **Normalized magnetization ($M(t)/M_0$) for different incident fluences onto the FM|Pt MLs.** The x-axis is linear up to 1 ps and logarithmic afterwards. Measured in out-of-plane geometry. Top: Fe|Pt ML, middle: Co|Pt ML, bottom: Ni|Pt ML

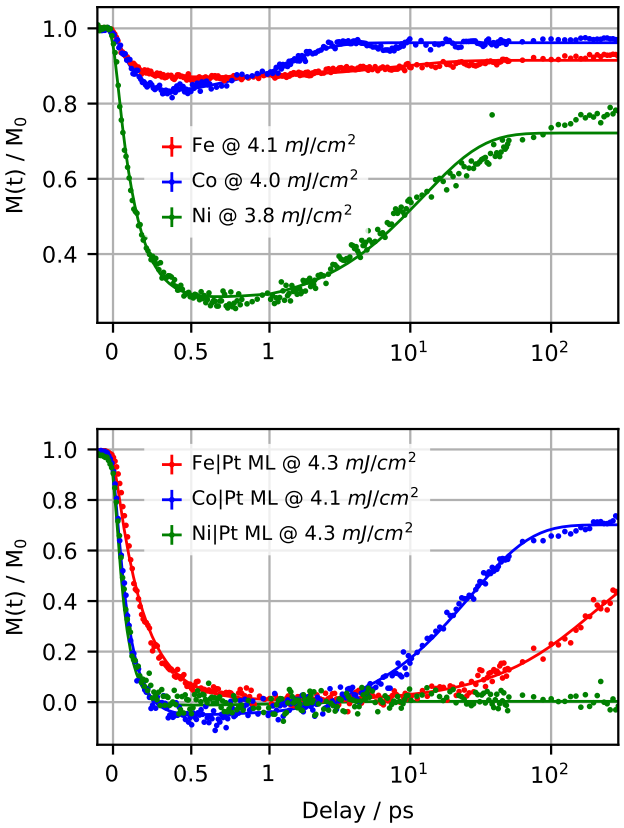

Figure 7. **Comparison of magnetization traces after laser excitation.** Normalized magnetization $(M(t)/M_0)$ for an absorbed fluence of $\approx 4\,\mathrm{mJ/cm^2}$. The x-axis is linear up to 1 ps and logarithmic afterwards. Dots are data points; lines are double exponential fits, as described in the text. Top: pure FMs, bottom: respective FM|Pt MLs.

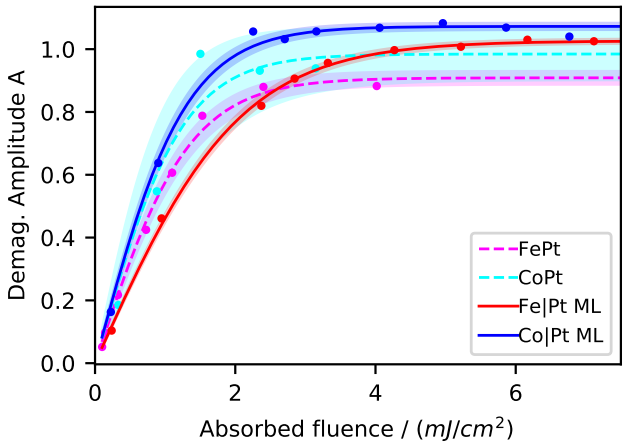

Figure 8. **Comparison of demagnetization amplitudes A of the alloys and multilayers (ML) of Fe|Pt and Co|Pt for a given absorbed fluence.** Data points as dots, linear-logistic fit as solid lines. For a given FM, the curves for alloys and MLs are similar within the margin of error at low fluences. At high fluences the MLs demagnetize slightly more than the alloys. Demagnetization of more than 100% is due to a normalization uncertainty.

	Γ_{exp} %/(mJ/cm^2)	Γ_{TDDFT} %/(mHa/a_0^3)
Fe	3.2 ± 0.1	7.4 ± 1.5
Co	7.3 ± 0.7	23.1 ± 7.2
Ni	23.7 ± 1.7	39.9 ± 9.7
FePt	58.1± 2.3	93 ± 16
CoPt	68 ± 14	124 ± 18
NiPt	—	185 ± 26
Fe|Pt ML	40.2 ± 3.5	—
Co|Pt ML	71.0 ± 2.3	—
Ni|Pt ML	120.3 ± 8.7	—

Table I. **Comparison of demagnetization efficiencies Γ.** Experimental values Γ_{exp} and simulated values Γ_{TDDFT}. NiPt is not ferromagnetic in the experiment. Values and errors are extracted from the linear-logistic fits described in the main text.

Here, θ is a step function centered at $t = \xi$ and the parameters A, B, τ_1, and τ_2 are the amplitudes and time scales of the de- and remagnetization, respectively. Since the remagnetization time constants strongly depend on the excitation fluence and will, consequently, influence early time dynamics differently, it is important to extract A and τ_1 via the above equation rather than reading them off from the curve's minimum. These fits are shown as solid lines in Figs. 4, 5, 6 and 7. For a brief discussion on the demagnetization constants we refer the reader to the supplementary Material[25]

The demagnetization amplitudes, A, for all investigated samples within a wide range of absorbed fluences are compared in Fig. 8 between the alloys and the multilayers and in Fig. 9 a) between the pure elements and the multilayers. For low fluences, we observe a linear relationship between absorbed fluence and A, while for higher fluences, as A approaches 100%, the induced changes begin to saturate. We model and fit this by a linear function, which transitions into a logistic function above its inflection point. We show the result as solid lines in Fig. 8 and Fig. 9 a), the colored error band corresponds to one standard deviation.

The slope of the linear part of this function, Γ, is a direct measure of the efficiency of the demagnetization process. We summarize the results for all samples in units of percent per given absorbed fluence in the first column of Tab. I. The uncertainties represent one standard deviation for the value, which we obtain from the least-square fit algorithm.

Interestingly, the pure FM's demagnetization efficiency follows the magnitude of the magnetic moment, instead of the material's Curie temperature, as often assumed in phenomenological three temperature models. Calculations based on the microscopic three temperature model[26] using tabulated values of the material constants predicts a more efficient demagnetization of Fe compared

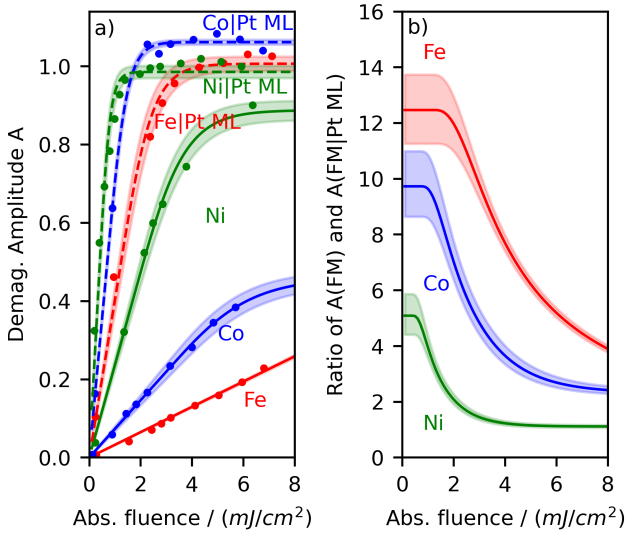

Figure 9. **Comparison of the experimental demagnetization amplitudes A.** a) Demagnetization amplitudes, A, of the FMs and their respective FM|Pt MLs are shown for a given absorbed fluence. The data has been fitted by the same linear-logistic function as used in Fig. 8. b) Ratios of A of each FM and A of their respective ML. This represents the magnitude of the change in demagnetization efficiency due to the presence of Pt in the MLs.

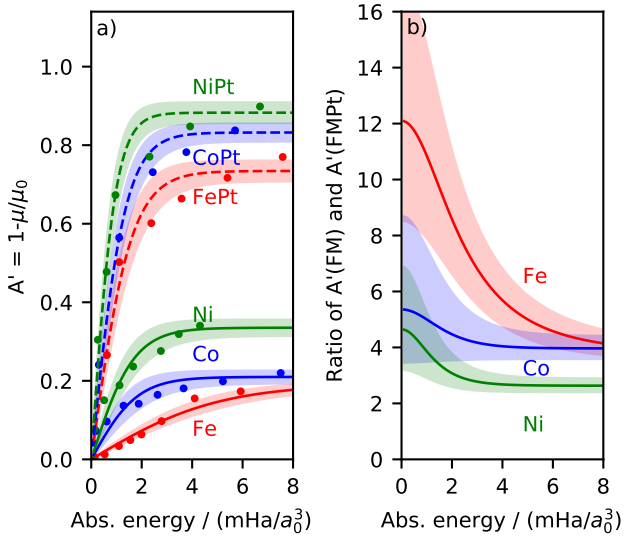

Figure 10. **Comparison of TDDFT results, showing the final magnetic moments μ after optical excitation.** a) Laser induced changes of the magnetic moment, $A' = 1 - \mu/\mu_0$, is shown as a function of the absorbed energy. The simulated data has been fitted by the same linear-logistic function as Fig. 9. b) Ratios defined as the quotient of A' of each FM and A' of their respective alloy. This represents the magnitude of the change in demagnetization efficiency due to the presence of Pt.

to Co, which we do not observe. We also like to note that, to our own surprise and to the best of our knowledge, this is the first time that all three *3d* transition metals, Fe, Co, and Ni are compared in a systematic experimental study under the same excitation conditions.

As we are interested in the increase in A between the pure FMs and the respective FM|Pt ML, we plot $A(\mathrm{FM|Pt})/A(\mathrm{FM})$ in Fig. 9 b). For low fluences, where A depends linearly on the absorbed energy for all samples, we can read off the relevant ratios: 12.5 ± 1.2 , 9.7 ± 1.1 and 5.1 ± 0.7 for Fe, Co and Ni, respectively. The colored error bands stem from the propagated uncertainties of the errors shown in Fig. 9 a).

V. EVALUATION AND DISCUSSION

Inspection of Figs. 8 and 9 allows us to make two important observations: first, the FM|Pt MLs, as well as the FMPt alloys demagnetize more efficiently than the corresponding pure FMs. Second, the increase of the demagnetization efficiency upon adding Pt to the pure FM corresponds very well to our hypothesis, put forward in Eq. 1: in Fe the ratio is 1.3±0.3 times larger compared to Co and 2.5±0.8 times larger compared to Ni. As a reminder, Fe inside FePt has a ≈1.4 times higher number of available, unoccupied states than Co inside CoPt and a ≈3.2 times higher number of available, unoccupied states than Ni inside NiPt.

Based on this observation, we suggest that the response of the FMPt compounds is mainly determined by OISTR and related to an efficient optical transfer of minority spins from Pt to the respective FM *3d* orbitals. Additionally, because the heavy metal Pt exhibits a high spin-orbit coupling, localized at the Pt atom, efficient spin-flips lead to the generation of additional minority electrons, which become available again for OISTR between Pt and the respective FM.

In order to further substantiate our hypothesis, we performed TDDFT simulations, using the Elk code[27]. For the pure FMs and their respective alloys we simulated the final magnetic moment, μ, 50 fs after the initial excitation. Beyond this time, the value for μ saturates as coupling to lattice dynamics and higher order scattering processes are ignored in TDDFT[28].

As the alloys and multilayers behave similarly experimentally, we can compare the simulations to the experimental data for alloys as well as to the data for the MLs. In Fig. 10 a), we present the simulated data: for better comparison to the experimental data, we show $A' = 1 - \mu/\mu_0$, where μ_0 is the magnetic moment of the saturated, unexcited state, as a function of the the absorbed energy per unit cell volume. (The units are milli Hartree, i.e. the atomic unit of energy, $\hbar/(m_e a_0^2)$, with $\hbar$ and m_e being the reduced Planck's constant and the electron mass respectively, per a_0^3, where a_0 is the classical Bohr radius.) One standard deviation between the fit and the

simulated data points is again represented by the colored bands.

The simulations show a linear trend for low energies, transitioning to a saturated demagnetization amplitude for higher energies, matching the response of the experimental data. The linear function again represents the demagnetization efficiency, Γ_{theo}, with units of percent demagnetization per given absorbed energy per unit volume. We present the values for Γ_{theo} in the second column of Tab. I.

The linear-logistic function, we use for fitting, shows larger deviations from the simulated data than for the experimental data. Therefore, the error bands are larger for the simulated than for the experimental data. Both these issues likely stem from the fact that the simulations only cover the first 50 fs and do not take any remagnetisation behavior into account. Despite these limitations, the TDDFT simulations reproduce the exact same trend as the experimental data: Fe demagnetizes the least efficient, followed by Co, Ni, FePt, CoPt, and finally NiPt. Most importantly, the calculated ratios of, A' for the FM and A of the FMPt alloys, as presented in Fig. 10 b), agree very well with the experimental data. For Fe we get a ratio of 12.0 ± 5.0, for Co 5.4 ± 3.3 and the smallest relative change for Ni of 4.6 ± 2.3.

A notable observation is that the saturation demagnetization amplitudes of the simulations are lower than those of the experimental data for all materials (with the exception of NiPt). This effect is most pronounced in pure Ni, where the experimental data shows more than 90% demagnetization at high fluences and the simulations stay below 40%. This is however due to the known fact that the presented TDDFT simulations do not account for the computationally very demanding memory effects (time dependence of electron-electron interaction) in the spin-flip part of the exchange-correlation kernel, which is used to calculated the final magnetic moments[29]. In Ni these effects are most pronounced and account for more than half the magnetic moment losses, which, if taken into account, would show a better agreement with the experimental data.

So far, we have concentrated our discussion on two microscopic mechanisms that drive the demagnetization and are included in our TDDFT calculations, namely spin-orbit mediated spin flips, as well as OISTR. However, there are other processes known to potentially influence the magnetization on an ultrafast time scale; in particular i) super-diffusive spin-transport [5,6] and ii) the generation of short wavelength magnons[30–32].

i) As lifetimes and velocities of excited electrons are known to depend on the band character of the excited electrons[33,34], superdiffusive spin currents may show a material- and therfore also a DOS-dependent response as well. To estimate a potential influence of this non-local process, we have calculated the depth-dependent energy absorption for all samples, taking into account the specific electric field distribution[35,36] within the hetero structures and using tabulated values of the optical constants[37]. We find comparable absorption profiles with very moderate excitation gradients on the order of 20% within the first 10 nm. Furthermore, in the FM|Pt MLs, we expect the mobility of majority carriers to be greatly reduced when crossing the respective Pt layers, because of a larger scattering probability in their localized, d-band electron states around the Fermi energy. The insulating substrates of all magnetic films further limit transport related effects. These arguments strongly suggest that our observations are not dominated by superdiffusive spin transport.

ii) The role of magnons in ultrafast demagnetization has been mostly inferred from a spectral analysis of optical MOKE[32] and resonant absorption measurements in the extreme ultraviolet[38–40] and soft X-ray spectral range[41] as well as from photo electron spectroscopy[30,42,43]. Observables proportional to the magnetization, which exhibit a response independent of the probing wavelength and are spectrally decoupled from electronic signals, are interpreted as fingerprints for the presence of transverse spin fluctuations. Generally, excitation of available spin wave states is governed by energy and momentum conservation and can therefore exhibit a material dependence, however, experimental evidence suggests that such delocalized spin excitations do not rely on specific non-thermal electron distributions but can be triggered by purely thermal effects[44] or superdiffusive spin currents[42] as well. Finally, we note that the good agreement between experiment and TDDFT calculations suggest that for early times after optical excitation, generation of magnons are not responsible for the observed differences of the demagnetization efficiency between pure elements and their respective FMPt alloys or FM|Pt multilayers . Therefore, we are convinced that our experimental results in conjunction with theoretical calculations, showing a scaling of the relative demagnetization amplitudes with the number of available, unoccupied minority states in the two component FMPt magnetic systems, are a direct confirmation of OISTR.

VI. CONCLUSION

In summary, we performed time-resolved P- and L-MOKE measurements to compare the demagnetization dynamics between pure ferromagnetic (FM) thin films Fe, Ni, and Co and respective FMPt alloys and FM|Pt multilayers. When adding Pt to any of the FMs, the demagnetization efficiency increases significantly and directly scales with the number of available, unoccupied states of the FM inside the ML. We experimentally verified that FePt and CoPt alloys show a very similar response compared to their respective MLs. Fe inside FePt has a ≈1.4 times higher number of available, unoccupied states than Co inside CoPt and a ≈3.2 times higher number of available, unoccupied states than Ni inside NiPt. The increase in efficiency between the FM and the FM|Pt ML exactly follows this trend: The ratio between Fe|Pt

& Fe is 1.3±0.3 times larger compared to Co & Co|Pt and 2.5±0.8 times higher than the one between Ni|Pt & Ni. Theoretical TDDFT simulations reproduce the experimentally determined relative demagnetization efficiencies for the pure elements, Fe, Co and Ni and are in good quantitative agreement with the relative increase of the demagnetization efficiency between the pure FM and the FMPt alloys.

In conclusion, these experimental findings further support the theory of optically induced intersite spin transfer (OISTR) and highlight its strong dependency on the number of available, unoccupied states. This opens up the path for tailoring demagnetization dynamics, based on DOS-engineering.

ACKNOWLEDGMENTS

We would like to thank DFG for funding through TRR227 projects A02 and A04. .

[1] E. Beaurepaire, J.-C. Merle, A. Daunois, and J.-Y. Bigot, Ultrafast Spin Dynamics in Ferromagnetic Nickel, Phys. Rev. Lett. **76**, 4250 (1996).

[2] C. D. Stanciu, F. Hansteen, A. V. Kimel, A. Kirilyuk, A. Tsukamoto, A. Itoh, and T. Rasing, All-Optical Magnetic Recording with Circularly Polarized Light, Phys. Rev. Lett. **99**, 047601 (2007).

[3] I. Radu, K. Vahaplar, C. Stamm, T. Kachel, N. Pontius, H. A. Dürr, T. A. Ostler, J. Barker, R. F. L. Evans, R. W. Chantrell, A. Tsukamoto, A. Itoh, A. Kirilyuk, T. Rasing, and A. V. Kimel, Transient ferromagnetic-like state mediating ultrafast reversal of antiferromagnetically coupled spins, Nature **472**, 205 (2011).

[4] K. Olejník, T. Seifert, Z. Kašpar, V. Novák, P. Wadley, R. P. Campion, M. Baumgartner, P. Gambardella, P. Němec, J. Wunderlich, J. Sinova, P. Kužel, M. Müller, T. Kampfrath, and T. Jungwirth, Terahertz electrical writing speed in an antiferromagnetic memory, Sci. Adv. **4**, eaar3566 (2018).

[5] M. Battiato, K. Carva, and P. M. Oppeneer, Superdiffusive Spin Transport as a Mechanism of Ultrafast Demagnetization, Phys. Rev. Lett. **105**, 027203 (2010).

[6] G. Malinowski, F. Dalla Longa, J. H. H. Rietjens, P. V. Paluskar, R. Huijink, H. J. M. Swagten, and B. Koopmans, Control of speed and efficiency of ultrafast demagnetization by direct transfer of spin angular momentum, Nature Physics **4**, 855 (2008).

[7] T. Kampfrath, M. Battiato, P. Maldonado, G. Eilers, J. Nötzold, S. Mährlein, V. Zbarsky, F. Freimuth, Y. Mokrousov, S. Blügel, M. Wolf, I. Radu, P. M. Oppeneer, and M. Münzenberg, Terahertz spin current pulses controlled by magnetic heterostructures, Nature Nanotechnology **8**, 256 (2013).

[8] T. J. Huisman, R. V. Mikhaylovskiy, J. D. Costa, F. Freimuth, E. Paz, J. Ventura, P. P. Freitas, S. Blügel, Y. Mokrousov, T. Rasing, and A. V. Kimel, Femtosecond control of electric currents in metallic ferromagnetic heterostructures, Nature Nanotechnology **11**, 455 (2016).

[9] T. Seifert, S. Jaiswal, U. Martens, J. Hannegan, L. Braun, P. Maldonado, F. Freimuth, A. Kronenberg, J. Henrizi, I. Radu, E. Beaurepaire, Y. Mokrousov, P. M. Oppeneer, M. Jourdan, G. Jakob, D. Turchinovich, L. M. Hayden, M. Wolf, M. Münzenberg, M. Kläui, and T. Kampfrath, Efficient metallic spintronic emitters of ultrabroadband terahertz radiation, Nature Photonics **10**, 483 (2016).

[10] T. Seifert, U. Martens, S. Günther, M. a. W. Schoen, F. Radu, X. Z. Chen, I. Lucas, R. Ramos, M. H. Aguirre, P. A. Algarabel, A. Anadón, H. S. Körner, J. Walowski, C. Back, M. R. Ibarra, L. Morellón, E. Saitoh, M. Wolf, C. Song, K. Uchida, M. Münzenberg, I. Radu, and T. Kampfrath, Terahertz Spin Currents and Inverse Spin Hall Effect in Thin-Film Heterostructures Containing Complex Magnetic Compounds, SPIN **07**, 1740010 (2017).

[11] J. K. Dewhurst, P. Elliott, S. Shallcross, E. K. U. Gross, and S. Sharma, Laser-Induced Intersite Spin Transfer, Nano Lett. **18**, 1842 (2018).

[12] J. Chen, U. Bovensiepen, A. Eschenlohr, T. Müller, P. Elliott, E. Gross, J. Dewhurst, and S. Sharma, Competing Spin Transfer and Dissipation at Co/Cu(001) Interfaces on Femtosecond Timescales, Phys. Rev. Lett. **122**, 067202 (2019).

[13] D. Steil, J. Walowski, F. Gerhard, T. Kiessling, D. Ebke, A. Thomas, T. Kubota, M. Oogane, Y. Ando, J. Otto, A. Mann, M. Hofherr, P. Elliott, J. K. Dewhurst, G. Reiss, L. Molenkamp, M. Aeschlimann, M. Cinchetti, M. Münzenberg, S. Sharma, and S. Mathias, Efficiency of ultrafast optically induced spin transfer in Heusler compounds, Phys. Rev. Research **2**, 023199 (2020).

[14] F. Siegrist, J. A. Gessner, M. Ossiander, C. Denker, Y.-P. Chang, M. C. Schröder, A. Guggenmos, Y. Cui, J. Walowski, U. Martens, J. K. Dewhurst, U. Kleineberg, M. Münzenberg, S. Sharma, and M. Schultze, Light-wave dynamic control of magnetism, Nature **571**, 240 (2019).

[15] P. Tengdin, C. Gentry, A. Blonsky, D. Zusin, M. Gerrity, L. Hellbrück, M. Hofherr, J. Shaw, Y. Kvashnin, E. K. Delczeg-Czirjak, M. Arora, H. Nembach, T. J. Silva, S. Mathias, M. Aeschlimann, H. C. Kapteyn, D. Thonig, K. Koumpouras, O. Eriksson, and M. M. Murnane, Direct light–induced spin transfer between different elements in a spintronic Heusler material via femtosecond laser excitation, Sci. Adv. **6**, eaaz1100 (2020).

[16] M. Hofherr, S. Häuser, J. K. Dewhurst, P. Tengdin, S. Sakshath, H. T. Nembach, S. T. Weber, J. M. Shaw, T. J. Silva, H. C. Kapteyn, M. Cinchetti, B. Rethfeld, M. M. Murnane, D. Steil, B. Stadtmüller, S. Sharma, M. Aeschlimann, and S. Mathias, Ultrafast optically induced spin transfer in ferromagnetic alloys, Sci. Adv. **6**, eaay8717 (2020).

[17] F. Willems, C. von Korff Schmising, C. Strüber, D. Schick, D. W. Engel, J. K. Dewhurst, P. Elliott, S. Sharma, and S. Eisebitt, Optical inter-site spin transfer probed by energy and spin-resolved transient absorption spectroscopy, Nat. Comm. **11**, 1 (2020).

[18] P. Elliott, N. Singh, K. Krieger, E. K. U. Gross, S. Sharma,

and J. K. Dewhurst, The microscopic origin of spin-orbit mediated spin-flips, Journal of Magnetism and Magnetic Materials **502**, 166473 (2020).

[19] K. C. Kuiper, T. Roth, A. J. Schellekens, O. Schmitt, B. Koopmans, M. Cinchetti, and M. Aeschlimann, Spin-orbit enhanced demagnetization rate in Co/Pt-multilayers, Appl. Phys. Lett. **105**, 202402 (2014).

[20] M. V. Lebedev, O. V. Misochko, T. Dekorsy, and N. Georgiev, On the nature of "coherent artifact", J. Exp. Theor. Phys. **100**, 272 (2005).

[21] N. Kawamiya and K. Adachi, Magnetic Properties of Ordered and Disordered Ni_(1-x) Fe_(x) Pt, J-Stage **16**, 327 (1975).

[22] See Supplementary Material at ... for hysteresis curves of all investigated samples.

[23] W. Zhang, P. Maldonado, Z. Jin, T. S. Seifert, J. Arabski, G. Schmerber, E. Beaurepaire, M. Bonn, T. Kampfrath, P. M. Oppeneer, and D. Turchinovich, Ultrafast terahertz magnetometry, Nat. Commun. **11**, 4247 (2020).

[24] Inspection of the oscillations of the Co data in Fig. 4 reveals a frequency of ≈150 GHz, corresponding to a time period of $6.\overline{6}$ ps. With the speed of sound in Co of ≈ 4.7 nm/ps this corresponds to a distance of ≈30 nm, i.e. twice the thickness of the sample. This suggests that the oscillations are most likely due to a acoustic strain wave launched upon laser excitation that couples to the magnetization. By changing the time range for the fitting algorithm, we confirmed that the oscillations do not influence the extracted values of A.

[25] See Supplementary Material at ... for details on the demagnetization time constants.

[26] B. Koopmans, G. Malinowski, F. Dalla Longa, D. Steiauf, M. Fähnle, T. Roth, M. Cinchetti, and M. Aeschlimann, Explaining the paradoxical diversity of ultrafast laser-induced demagnetization, Nat. Mat. **9**, 259 (2010).

[27] J. K. Dewhurst and S. Sharma, The Elk Code (2018).

[28] K. Krieger, J. K. Dewhurst, P. Elliott, S. Sharma, and E. K. U. Gross, Laser-Induced Demagnetization at Ultrashort Time Scales: Predictions of TDDFT, J. Chem. Theory Comput. **11**, 4870 (2015).

[29] S. R. Acharya, V. Turkowski, G. Zhang, and T. S. Rahman, Ultrafast Electron Correlations and Memory Effects at Work: Femtosecond Demagnetization in Ni, Phys. Rev. Lett. **125**, 017202 (2020).

[30] A. B. Schmidt, M. Pickel, M. Donath, P. Buczek, A. Ernst, V. P. Zhukov, P. M. Echenique, L. M. Sandratskii, E. V. Chulkov, and M. Weinelt, Ultrafast Magnon Generation in an Fe Film on Cu(100), Phys. Rev. Lett. **105**, 197401 (2010).

[31] E. Carpene, E. Mancini, C. Dallera, M. Brenna, E. Puppin, and S. De Silvestri, Dynamics of electron-magnon interaction and ultrafast demagnetization in thin iron films, Phys. Rev. B **78**, 174422 (2008).

[32] E. Carpene, H. Hedayat, F. Boschini, and C. Dallera, Ultrafast demagnetization of metals: Collapsed exchange versus collective excitations, Phys. Rev. B **91**, 174414 (2015).

[33] M. Bauer and M. Aeschlimann, Dynamics of excited electrons in metals, thin films and nanostructures, Journal of Electron Spectroscopy and Related Phenomena Frontiers in photoemission spectroscopy of solids and surfaces, **124**, 225 (2002).

[34] V. P. Zhukov, E. V. Chulkov, and P. M. Echenique, Lifetimes and inelastic mean free path of low-energy excited electrons in Fe, Ni, Pt, and Au: Ab initio GW+T calculations, Phys. Rev. B **73**, 125105 (2006).

[35] D. L. Windt, IMD—Software for modeling the optical properties of multilayer films, Computers in Physics **12**, 360 (1998).

[36] A. R. Khorsand, M. Savoini, A. Kirilyuk, and T. Rasing, Optical excitation of thin magnetic layers in multilayer structures, Nature Materials **13**, 101 (2014).

[37] E. D. Palik, *Handbook of Optical Constants of Solids* (Academic Press, 1998).

[38] D. Zusin, P. M. Tengdin, M. Gopalakrishnan, C. Gentry, A. Blonsky, M. Gerrity, D. Legut, J. M. Shaw, H. T. Nembach, T. J. Silva, P. M. Oppeneer, H. C. Kapteyn, and M. M. Murnane, Direct measurement of the static and transient magneto-optical permittivity of cobalt across the entire M-edge in reflection geometry by use of polarization scanning, Phys. Rev. B **97**, 024433 (2018).

[39] E. Turgut, D. Zusin, D. Legut, K. Carva, R. Knut, J. M. Shaw, C. Chen, Z. Tao, H. T. Nembach, T. J. Silva, S. Mathias, M. Aeschlimann, P. M. Oppeneer, H. C. Kapteyn, M. M. Murnane, and P. Grychtol, Stoner versus Heisenberg: Ultrafast exchange reduction and magnon generation during laser-induced demagnetization, Phys. Rev. B **94**, 220408 (2016).

[40] S. Jana, R. S. Malik, Y. O. Kvashnin, I. L. M. Locht, R. Knut, R. Stefanuik, I. Di Marco, A. N. Yaresko, M. Ahlberg, J. Åkerman, R. Chimata, M. Battiato, J. Söderström, O. Eriksson, and O. Karis, Analysis of the linear relationship between asymmetry and magnetic moment at the M edge of 3d transition metals, Phys. Rev. Research **2**, 013180 (2020).

[41] D. J. Higley, A. H. Reid, Z. Chen, L. L. Guyader, O. Hellwig, A. A. Lutman, T. Liu, P. Shafer, T. Chase, G. L. Dakovski, A. Mitra, E. Yuan, J. Schlappa, H. A. Dürr, W. F. Schlotter, and J. Stöhr, Femtosecond X-ray induced changes of the electronic and magnetic response of solids from electron redistribution, Nature Communications **10**, 5289 (2019).

[42] S. Eich, M. Plötzing, M. Rollinger, S. Emmerich, R. Adam, C. Chen, H. C. Kapteyn, M. M. Murnane, L. Plucinski, D. Steil, B. Stadtmüller, M. Cinchetti, M. Aeschlimann, C. M. Schneider, and S. Mathias, Band structure evolution during the ultrafast ferromagnetic-paramagnetic phase transition in cobalt, Science Advances **3**, e1602094 (2017).

[43] R. Gort, K. Bühlmann, S. Däster, G. Salvatella, N. Hartmann, Y. Zemp, S. Holenstein, C. Stieger, A. Fognini, T. Michlmayr, T. Bähler, A. Vaterlaus, and Y. Acremann, Early Stages of Ultrafast Spin Dynamics in a 3d Ferromagnet, Phys. Rev. Lett. **121**, 087206 (2018).

[44] G. Salvatella, R. Gort, K. Bühlmann, S. Däster, A. Vaterlaus, and Y. Acremann, Ultrafast demagnetization by hot electrons: Diffusion or super-diffusion?, Structural Dynamics **3**, 055101 (2016).